國立臺灣大學理學院物理研究所

碩士論文

Department of Physics

College of Science

National Taiwan University

Master's Thesis

使用可調耦合器校準控制-Z 閘以實現超過 96% 的保真度

Calibration of CZ Gate with Tunable Coupler to Achieve Fidelity Above 96%

謝博安

Po-An Hsieh

指導教授: 管希聖 博士

Advisor: Hsi-Sheng Goan Ph.D.

中華民國 114 年 7 月

July, 2025

doi:10.6342/NTU202501389

Acknowledgements

Thank for professor Goan, professor Chen and all the members in the lab.

doi:10.6342/NTU202501389

doi:10.6342/NTU202501389

摘要

隨著單一量子位元量子邏輯閘的保真度已經趨於完美，針對兩個量子位元的操作與量子邏輯閘的保真度將成為下一個重要的議題。由於兩個量子位元間存在ZZ-交互作用，除了降低原本單一量子位元邏輯閘的保真度，也使兩個量子位元邏輯閘的操作受到限制。為了使兩個量子位元間的相互影響可以受到控制，量子耦合器成為不可或缺的角色。在這篇論文中我們首先要了解量子耦合器的性質，再來利用它建立且校準控制-Z 閘，並藉由兩個量子位元的隨機標竿分析法來計算控制-Z 閘的保真度。

關鍵字：控制-Z 閘、量子耦合器、保真度

doi:10.6342/NTU202501389

doi:10.6342/NTU202501389

Abstract

As the fidelity of single-qubit quantum logic gates approaches perfection, the focus of quantum gate optimization has shifted to two-qubit operations. The fidelity of two-qubit gates has become a critical issue. Due to the presence of ZZ interactions between qubits, not only is the fidelity of single-qubit gates decreased, but the performance of two-qubit gates is also significantly limited. To mitigate and control the mutual interactions between qubits, quantum couplers have become an indispensable component. In this work, we first investigate the properties of tunable quantum couplers. We then utilize the coupler to construct and calibrate a Controlled-Z (CZ) gate, and evaluate its performance using two-qubit randomized benchmarking to determine the fidelity of the CZ gate.

Keywords: CZ gate, Coupler, Fidelity

doi:10.6342/NTU202501389

doi:10.6342/NTU202501389

Contents

doi:10.6342/NTU202501389

doi:10.6342/NTU202501389

List of Figures

doi:10.6342/NTU202501389

doi:10.6342/NTU202501389

doi:10.6342/NTU202501389

doi:10.6342/NTU202501389

doi:10.6342/NTU202501389

doi:10.6342/NTU202501389

List of Tables

doi:10.6342/NTU202501389

doi:10.6342/NTU202501389

Chapter 1

Introduction

In order to get high fidelity of two qubits gate, tunable couplers have been more popular in nowadays quantum interconnect hardware. Although they are tools to control the interaction between qubits and they are designed not to be excited in two qubits operation, knowing the properties of couplers still have some benefits. For one qubit there are three supporting components like readout circuit, flux line and XY line. It costs hardware overhead if coupler has all dedicated components like qubit, so coupler only has its flux line. Then, precisely characterizing coupler becomes challenge without such components. One method is that borrow the readout resonator from neighboring qubit. Since the weak coupling strength between nearby resonator and coupler itself, the duration of readout pulse should be rather long, causing decoherence.

There is a robust approach to characterize tunable couplers accurately based on adiabatic control, which also called adiabatic swap (aSWAP). This approach first swaps the states between the coupler and the neighboring qubit adiabatically and utilizes the strong coupling strength between qubit and resonator to readout the state of the coupler. Using this method, basic properties of coupler such that frequency, T1 and T2 at arbitrary flux

doi:10.6342/NTU202501389

bias can be easily measured. Coupler frequency can help us to calculate the residual ZZ-interaction between two qubits. And we also can estimate our two qubits gate coherence limit with coupler decoherence time.

Two qubit gates, especially CZ gate, can be calibrated in real experiment using Z gate of qubits. With a tunable coupler between two qubits, the ZZ-interaction between two neighboring qubits can be adjusted by tuning the frequency of the coupler. It is expected that the ZZ-interaction is zero when performing single qubit operations and turns on the strong interaction while doing two-qubit operations. One common way to check the defect of CZ gate is randomized benchmarking (RB). Since RB averages quantum circuits generated randomly and evaluates the gate fidelity by decay rate of gate error, it does not need high readout fidelity.

In the first part of this thesis we introduce some theoretical concept for the operation to two-qubit with one coupler. In the second part we demonstrate how to use adiabatic swap in experiments to get coupler basic parameters and the experimental method of calibrating the CZ gate. In the forth part of this thesis we use randomized benchmarking to examine the fidelity of our CZ gate. Finally, we conclude what we have done and discuss possible improvements in the future.

doi:10.6342/NTU202501389

Chapter 2

Theoretical background

In this chapter, we introduce the concept of adiabatic swap and some operations to two qubits with one tunable coupler.

2.1 Adiabatic Swap (aSWAP)

When the coupler frequency is far detuned from qubits, the hybridization between the three elements can be ignored. As the frequency of the coupler is close to that of qubits, their states strongly hybridize, and degeneracy occurs around the resonance, as shown in Figure 2.1. According to the adiabatic theorem, when the coupler is tuned slowly enough by its flux sweep, any eigenstate keeps in the instant eigenstate [1]. The ”slowly enough” is determined by the coupling strength between the qubit and the coupler. Take the multiplicative inverse of coupling strength is the period of state exchange between two elements when they are on resonance. Therefore, the length of tuning the coupler should be longer than this period and we assume it to be adiabatic. So, if the coupler stays in an excited state initially, when it goes through the degeneracy region by the flux sweep

doi:10.6342/NTU202501389

adiabatically, the states swap between the coupler and the qubit, as shown in Figure 2.1.

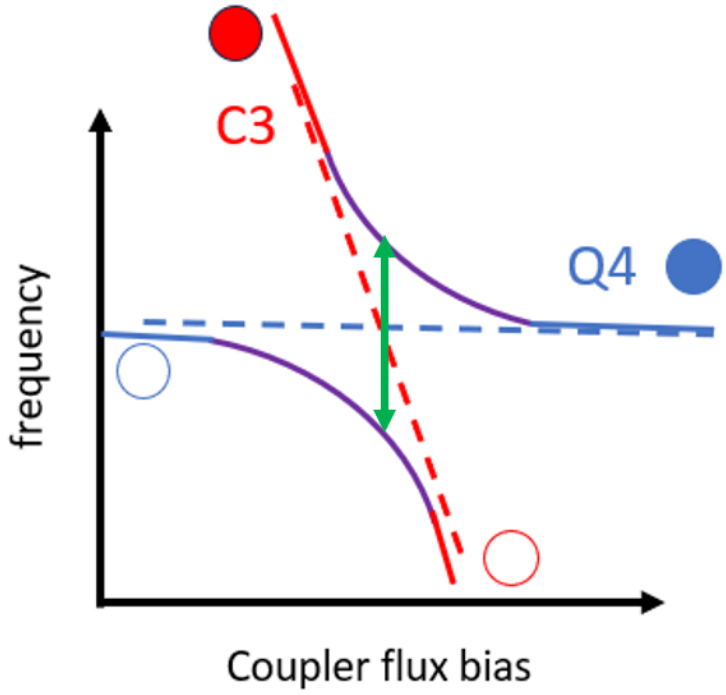

Figure 2.1: Schematic diagram of two circumstances when coupler pass through qubit by its magnetic flux. The dashed lines represent the bare energy levels of the coupler (red) and the qubit (blue). Strong coupling between the coupler and the qubit that hybridizes their states and causes degeneracy, leads to the spectrum of dressed state (solid line). The filled and hollow circle indicate excited state and ground state. The green arrow indicates the coupling strength between the qubit and the coupler. In the diagram we set coupler is in excited state initially.

Using aSWAP has some advantages. One is pulse length robustness, as mentioned before, if the frequency of the coupler is tuned ”slowly” enough that can make the process to be adiabatic, more slower of the tuning is allowed. Thus, this method is time-invariant. This is opposite to another swapping method, iswap, which exchanges the states between the coupler and the qubit depending on time. The other advantage is that the readout signal is as clear as the qubit measurement before. Since the states exchange between the coupler and the qubit and there is strong coupling between the qubit and the resonator, it looks no difference when measuring the coupler.

doi:10.6342/NTU202501389

2.2 Single qubit gate

The basic operations for single qubit in matrix form is

$$I = \begin{pmatrix} 1 & 0 \\ 0 & 1 \end{pmatrix}, \; X = \begin{pmatrix} 0 & 1 \\ 1 & 0 \end{pmatrix},$$

$$Y = \begin{pmatrix} 0 & -i \\ i & 0 \end{pmatrix}, \; Z = \begin{pmatrix} 1 & 0 \\ 0 & -1 \end{pmatrix}, \tag{2.1}$$

each of which represents rotating 180 degree along the corresponding axis of the Bloch Sphere. There are four more important operations that make $|0\rangle$ lies on the equator of the Bloch Sphere, that is

$$X/2 = \frac{1}{\sqrt{2}} \begin{pmatrix} 1 & -i \\ -i & 1 \end{pmatrix}, \; Y/2 = \frac{1}{\sqrt{2}} \begin{pmatrix} 1 & -1 \\ 1 & 1 \end{pmatrix},$$

$$-X/2 = \frac{1}{\sqrt{2}} \begin{pmatrix} 1 & i \\ i & 1 \end{pmatrix}, \; -Y/2 = \frac{1}{\sqrt{2}} \begin{pmatrix} 1 & 1 \\ -1 & 1 \end{pmatrix}. \tag{2.2}$$

According to Eq 2.1, Z can be written in terms of X, Y,

$$Z = \begin{pmatrix} 1 & 0 \\ 0 & -1 \end{pmatrix} = -i \begin{pmatrix} 0 & 1 \\ 1 & 0 \end{pmatrix} \begin{pmatrix} 0 & -i \\ i & 0 \end{pmatrix} = -iXY \tag{2.3}$$

. Thus, we can establish a Clifford group using $\{I, X, Y, X/2, Y/2, -X/2, -Y/2\}$. Clifford gates are quantum logic gates that map Pauli operators (X, Y, Z) to other Pauli operators under conjugation. In other words, let C be the Clifford group for single qubit and P be the Pauli group associated with four Pauli matrix in Eq 2.1 with phases $\{\pm 1, \pm i\}$, for

doi:10.6342/NTU202501389

Single Qubit Cliffords	
Paulis	I
	X
	Y
	Y, X
$\pi/2$ rotations	$X/2$
	$-X/2$
	$Y/2$
	$-Y/2$
	$-X/2, Y/2, X/2$
	$-X/2, -Y/2, X/2$
$2\pi/3$ rotations	$X/2, Y/2$
	$X/2, -Y/2$
	$-X/2, -Y/2$
	$-X/2, -Y/2$
	$Y/2, X/2$
	$Y/2, -X/2$
	$-Y/2, X/2$
	$-Y/2, -X/2$
Hardamard-like	$X, Y/2$
	$X, -Y/2$
	$Y, X/2$
	$Y, -X/2$
	$X/2, Y/2, X/2$
	$-X/2, Y/2, -X/2$

Table 2.1: Single qubit Clifford group. These 24 Clifford gates can be divided into four categories according to their appearence.

any unitary operation U that $U \in C$ if $UpU^\dagger \in P$ for all $p \in P$ [2]. There are 24 Clifford gates in Clifford group for single qubit and we can separate them into four categories, as shown in table 2.1.

2.3 ZZ-interaction

In qubit-qubit (Q-Q) system, the static ZZ-interaction is defined as

$$\zeta = \omega_{11} - \omega_{01} - \omega_{10} + \omega_{00} \tag{2.4}$$

doi:10.6342/NTU202501389

where the ω represents the eigenstate of the Q-Q system and the subscript indicates the state of each qubit. In order to have the ability to adjust the ZZ-interaction in favor of the two-qubit operations, the coupler is placed between two qubits. In this case, the Q-C-Q system need to be considered now rather than the Q-Q system. The coupler is expected to be the role that closes the ZZ-interaction when the single-qubit operations work and opens the ZZ-interaction when it comes to two-qubit operations. The ZZ-interaction can be eliminated if the detuning between two qubits is less than their anharmonicity, $\Delta = |\omega_1 - \omega_2| \in [\alpha_2, -\alpha_1]$ where ω_i and α_i represent the frequency and the anharmonicity of qubit i [3]. Under this condition, the ZZ-interaction can be calculated from

$$ZZ^{(1)} = 2g_{12}^2 \left[\frac{1}{\Delta_{12} - \alpha_2} - \frac{1}{\Delta_{12} + \alpha_1} \right] \tag{2.5}$$

$$ZZ^{(2)} = 2g_{12}g_{1c}g_{2c} \left[\frac{2}{(\Delta_{12} - \alpha_2)\Delta_1} - \frac{2}{(\Delta_{12} + \alpha_1)\Delta_2} + \frac{2}{\Delta_1\Delta_2} \right] \tag{2.6}$$

$$ZZ^{(3)} = 2g_{1c}^2 g_{2c}^2 \left[\frac{1}{\Delta_1^2(\Delta_{12} - \alpha_2)} - \frac{1}{\Delta_2^2(\Delta_{12} + \alpha_1)} + \frac{1}{\Delta_1 + \Delta_2 - \alpha_c} \left(\frac{1}{\Delta_1} + \frac{1}{\Delta_2} \right)^2 \right] \tag{2.7}$$

$$\zeta = ZZ^{(1)} + ZZ^{(2)} + ZZ^{(3)} \tag{2.8}$$

where Δ_{12}, Δ_1, Δ_2 represent the detuning between qubits or the qubit and the coupler, g_{12}, g_{1c}, g_{2c} are the coupling strength between qubits or the qubit and the coupler [4]. The residual ZZ-interaction Eq 2.8 is the summation from Eq 2.5 to Eq 2.7.

doi:10.6342/NTU202501389

2.4 CZ gate

One basic two-qubit gate is the Control-Z gate (CZ gate). The matrix form is expressed in

$$CZ = \begin{pmatrix} 1 & 0 & 0 & 0 \\ 0 & 1 & 0 & 0 \\ 0 & 0 & 1 & 0 \\ 0 & 0 & 0 & -1 \end{pmatrix} \tag{2.9}$$

in the basis of

$$|00\rangle = \begin{pmatrix} 1 \\ 0 \\ 0 \\ 0 \end{pmatrix}, |01\rangle = \begin{pmatrix} 0 \\ 1 \\ 0 \\ 0 \end{pmatrix}, |10\rangle = \begin{pmatrix} 0 \\ 0 \\ 1 \\ 0 \end{pmatrix}, |11\rangle = \begin{pmatrix} 0 \\ 0 \\ 0 \\ 1 \end{pmatrix}. \tag{2.10}$$

The CZ gate operates on the four states in Eq 2.10 remaining the same except $|11\rangle$ with an additional minus sign. The minus sign indicates that the phase has changed. This feature is the most important but also difficult when constructing the CZ gate in real experiment.

From the above discussion, finding a way to let $|11\rangle$ become $-|11\rangle$ in real experiment is the key to establish the CZ gate. Considering the eigenfrequencies of the Q-Q system, the neighboring states of $|11\rangle$ are $|20\rangle$ and $|02\rangle$ [5]. Since the eigenfrequency of the transmon qubit is tunable, if $|11\rangle$ and $|20\rangle$ are on resonance, the eigenstate of the system swaps between $|11\rangle$ and $|20\rangle$ along with the evolution time and the additional factor i appears when the swapping completes once. So, $|11\rangle$ returns to itself but obtains a factor -1, which is highly desired for the CZ gate. That is the concept of constructing the CZ

doi:10.6342/NTU202501389

gate in real case.

2.5 Randomized Benchmarking

In this section, we introduce the Single-Qubit RB and Two-Qubit RB separately.

2.5.1 Single-Qubit Randomized Benchmarking

Below are the experimental steps of SQRB:

1. Prepare the qubit at the ground state initially.
2. Apply a sequence of m Clifford gates from Table 2.1 to the qubit.
3. Apply an additional (m+1)th gate which inverts the whole sequence. As we established above , this inverse gate can be found in the Clifford group (Table 2.1).
4. Measure the probability of the resulting ground state.
5. Change the component of the sequence and repeat the step 2-4 k times.
6. Repeat for multiple lengths m to build up an exponential decay.

The fitting function of the SQRB is

$$F_{seq} = Ap_{ref}^{m} + B, \tag{2.11}$$

where A, B are some constants and p_{ref} is the decay constant obtained from the exponential fitting. The error of per Clifford gate is

$$r_{ref} = \frac{(1 - p_{ref})(d - 1)}{d}, d = 2^{N}, \tag{2.12}$$

doi:10.6342/NTU202501389

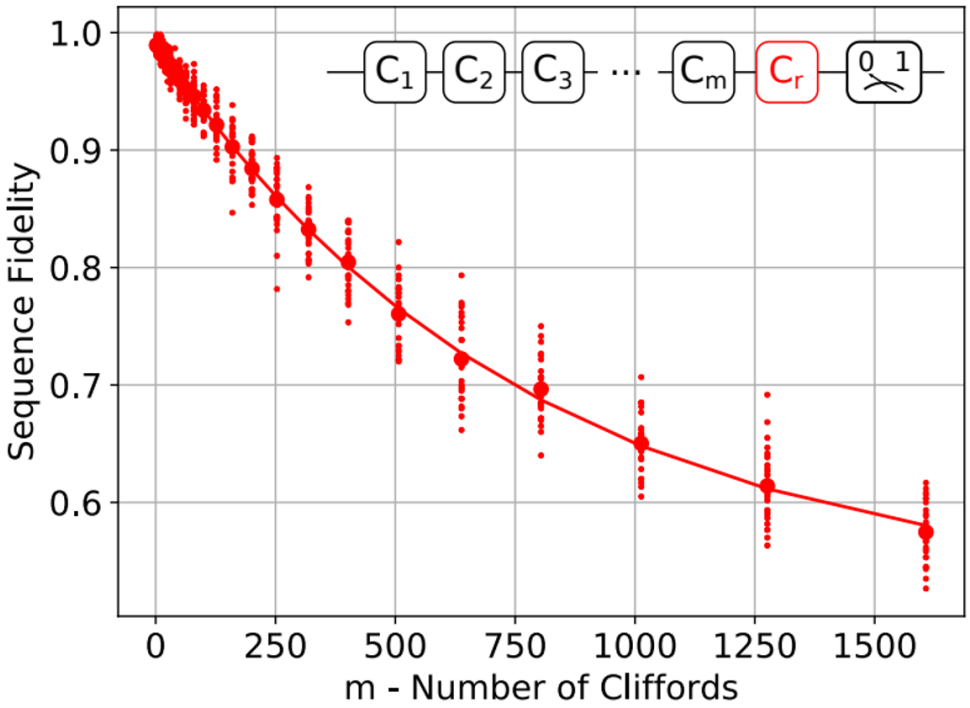

Figure 2.2: The schematic diagram of the result from SQRB. The inset shows that apply m Clifford gates initially and then apply an inverse gate to make the qubit to the ground state. By changing the number of Clifford gate in the sequence, the result is expected to be an exponential decay relative to the population of the ground state.

where N is the number of the qubit. And the gate fidelity result from SQRB is

$$F_{ref} = 1 - r_{ref}. \tag{2.13}$$

Actually, there are 45 physical gates consisting of 24 Clifford gates for single qubit. Thus, the average physical gate fidelity is

$$F_{avg} = 1 - \frac{r_{ref}}{1.875}. \tag{2.14}$$

2.5.2 Two-Qubit Randomized Benchmarking

The two-qubit Clifford group contains four classes:

1. The single qubit class (Figure 2.3a)

doi:10.6342/NTU202501389

2. The SWAP-like class (Figure 2.3b)

3. The iSWAP-like class (Figure 2.3c)

4. The CNOT-like class (Figure 2.3d)

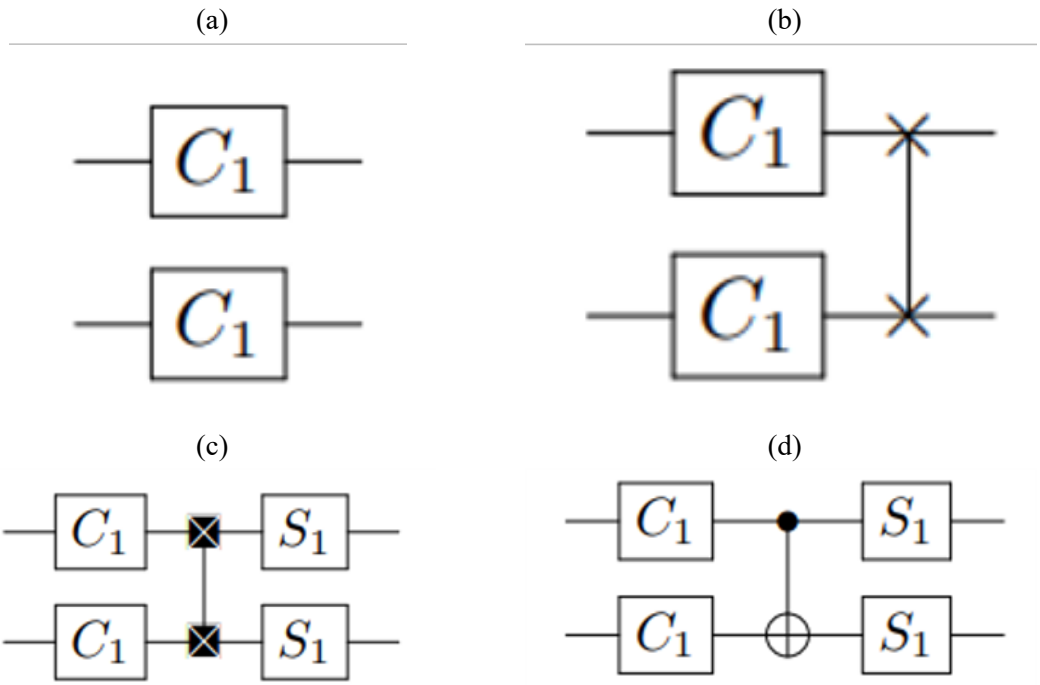

Figure 2.3: The quantum circuit of the four classes in two-qubit Clifford group. (a) The single qubit class. (b) The SWAP-like class. (c) The iSWAP-like class. (d) The CNOT-like class.

From Figure 2.3, it is obvious that we need C_1 group and $S1$ group to help us construct the two-qubit Clifford group. The C_1 group indicates the single-qubit Clifford group as shown before (Table 2.1). The S_1 group consists of the operators that rotate the Bloch sphere to exchange all the axes. There are three members in S_1 group:

Single Qubit Cliffords	
S_1	I
	$Y/2, X/2$
	$-X/2, -Y/2$

Table 2.2: Three gates in S_1 group.

So, the single qubit class has $24^2 = 576$ elements, the SWAP-like class consists of

doi:10.6342/NTU202501389

$24^2 = 576$ elements, the iSWAP-like class has $24^2 * 3^2 = 5184$ elements and the CNOT-like class consists of $24^2 * 3^2 = 5184$ elements. The total number of the Clifford gates in two-qubit Clifford group is 11520 [6]!

There is another issue that needs to be taken into account. Although the two-qubit gates in the middle of Figure 2.3b, Figure 2.3c, Figure 3.2 are not CZ gate, they can be fabricated by the CZ gate and single qubit gates, as shown below:

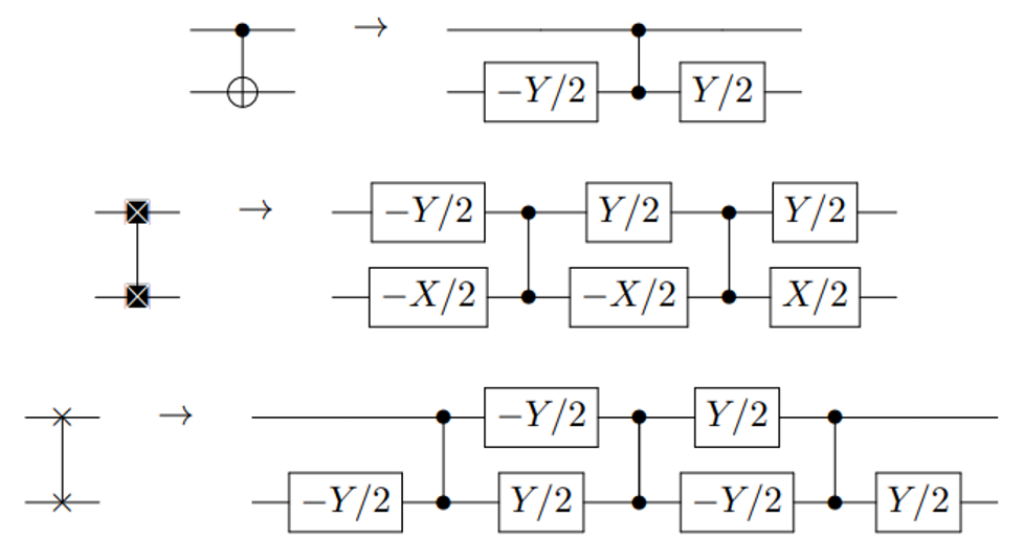

Figure 2.4: Rewrite the CNOT, iSWAP, SWAP gate in terms of CZ gate and single qubit gates.

The experimental steps and the fitting fuction for TQRB are the same as SQRB.

The error of per two-qubit Clifford gate r_{C_2} can be calculated from the error of per single qubit Clifford gate r_{C_1} and the error of the CZ gate. According to the discussion in 2.5.1, $r_{C_1} = \frac{45}{24} r_{SQ}$, the error resulting from the four classes of two-qubit Clifford group can be listed separately.

The single qubit class:

$$r_{C_1 \otimes C_1} = \frac{90}{24} r_{SQ} \tag{2.15}$$

doi:10.6342/NTU202501389

The SWAP-like class:

$$r_{SWAP} = 3r_{CZ} + \frac{35}{4}r_{SQ} \tag{2.16}$$

The iSWAP-like class:

$$r_{iSWAP} = 2r_{CZ} + \frac{113}{12}r_{SQ} \tag{2.17}$$

The CNOT-like class:

$$r_{CNOT} = r_{CZ} + \frac{89}{12}r_{SQ}. \tag{2.18}$$

So, the error of per two-qubit Clifford gate is

$$\begin{aligned} r_{C_2} &= \frac{576}{11520}r_{C_1\otimes C_1} + \frac{576}{11520}r_{SWAP} + \frac{5184}{11520}r_{iSWAP} + \frac{5184}{11520}r_{CNOT} \\ &= \frac{3}{2}r_{CZ} + \frac{33}{4}r_{SQ}. \end{aligned} \tag{2.19}$$

Eq 2.19 also indicates that per two-qubit Clifford gate contains 8.25 single gates and 1.5 CZ gates [7].

doi:10.6342/NTU202501389

doi:10.6342/NTU202501389

Chapter 3

Experiment process

3.1 Experiment setup

Below are the two chips used in the following experiment. The design of these two chips are the same. Both with five tunable qubits and four tunable couplers between the neighboring qubits. Chip A is used in 3.2 for demonstrating the method to characterize

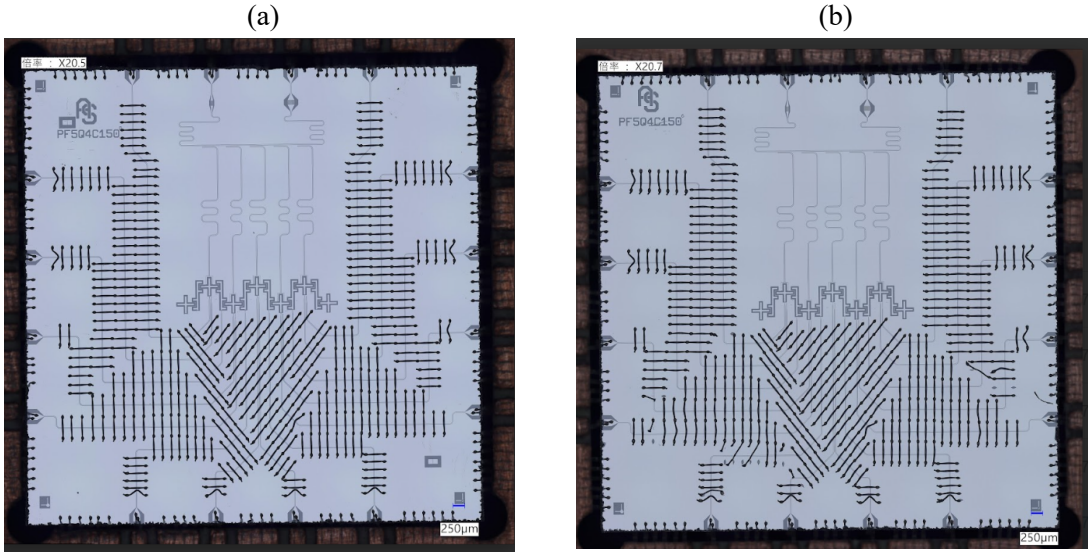

Figure 3.1: (a) The full image of Chip A. (b) The full image of Chip B

the coupler without dedicated resonator. We select the two qubits and one coupler on the

doi:10.6342/NTU202501389

right hand side for the following experiments. Chip B is used in 3.3 for constructing the CZ gate and measuring the gate fidelity. We pick two qubits and one coupler in the middle of the chip labeled as Q_1, Q_2 and C in the experiment of CZ gate calibration. The reason that not using a chip for the coupler characterization and CZ gate construction is the qubits in chip A are not tunable and it is impossible to construct the CZ gate. Therefore, we take another chip to complete the experiments.

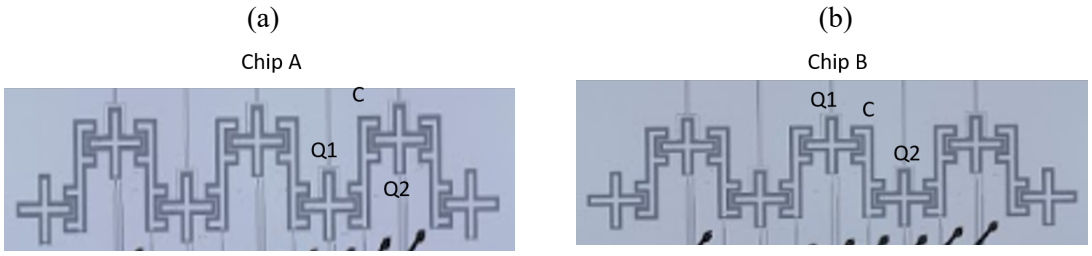

Figure 3.2: The enlarge image of Chips (a) We use Q_1-C-Q_2 system on the right hand side for coupler characterization. (b) The Q_1-C-Q_2 system is used to calibrate the CZ gate.

3.2 Coupler Characterization with aSWAP

According to the above discussion, it is obvious that finding the anti-crossing point of the qubit and the coupler is important for the aSWAP method.

3.2.1 Qubit characterization and Anti-crossing point identification

Before studying the coupler, the basic thing to do is identifying the frequency of the qubit. We first recognize the frequency of the Q_2 via two-tone measurement, the experiment pulse sequence is shown in Figure 3.3a. We give a long driving pulse varying the driving frequency through the XY line to Q_2. When driving frequency is equal to the resonant frequency of Q_2, the readout signal emerges a peak at 4.749 GHz in the spectrum (Figure 3.3c, then we obtain the frequency of Q_2 is now 4.749 GHz. Since the frequency

doi:10.6342/NTU202501389

of qubit is tunable by its magnetic flux and it is expected to be maximum in our following experiments, we execute the flux two-tone measurement to check whether Q_2 is at its sweet spot (Figure 3.3b). Different from the two-tone measurement, we give a long flux bias to Q_2 with driving pulse simultaneously. So the result should exhibit the frequency of Q_2 at arbitrary flux bias. From Figure 3.3d we can observe that the frequency of Q_2 is non-tunable by magnetic flux. Although in transmon qubit design the spectrum should be hyperbola rather than a straight line, this feature still gives the advantage that we can neglect the flux crosstalk resulting from the neighboring coupler.

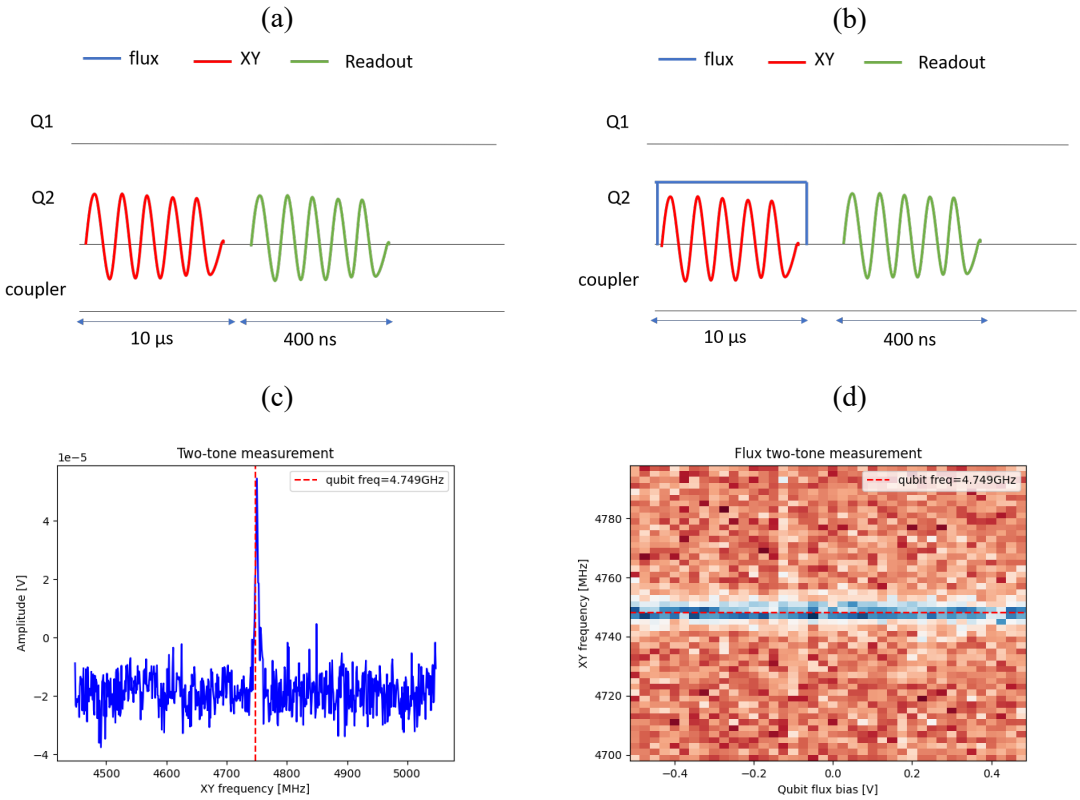

Figure 3.3: (a) The pulse sequence of the two-tone measurement. (b) The pulse sequence of the flux two-tone measurement. (c) The result of the two-tone measurement. (d) The result of the flux two-tone measurement. The red color means Q_2 stays in ground state, blue means Q_2 is excited by driving pulse pumping with specific frequency.

After identifying the frequency of Q_2, the next step is confirming the anti-crossing point of Q_2 and the coupler. So we execute another flux two-tone measurement. But this time we apply magnetic flux to the coupler instead of Q_2 (Figure 3.4a). Thus, the fre-

doi:10.6342/NTU202501389

quency of the coupler can be tuned down to approach Q_2. The result spectrum is expected to be the same as the solid line in Figure 2.1. From Figure 3.4b we know that the coupler

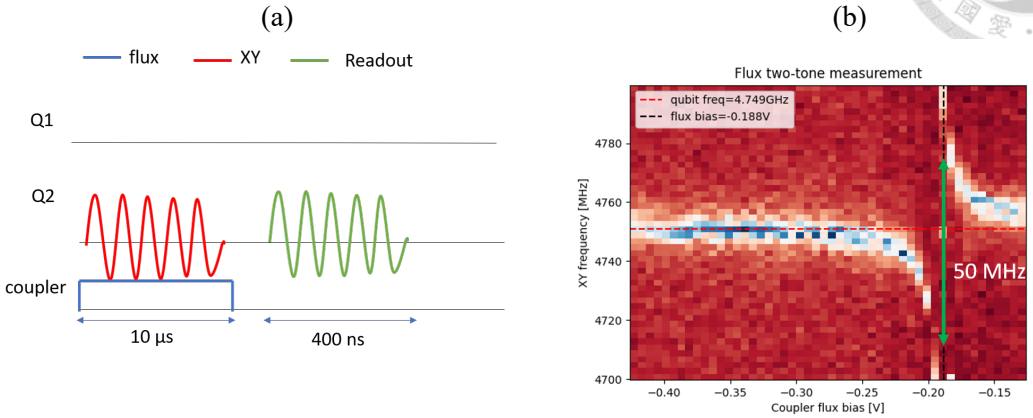

Figure 3.4: (a) The pulse sequence of the flux two-tone measurement. Driving a long pulse in the XY line of Q_2 and a magnetic square wave in the Z line of the coupler simultaneously. Altering the amplitude of the magnetic wave and the pumping frequency of the driving pulse as parameters, this measurement is expected to tell a certain bias that coupler collides with Q_2 at. (b) The x-axis is the flux bias of the coupler, the y-axis is the pumping frequency in driving pulse. It is obvious that coupler collides with qubit at -0.188 V. The coupling strength is 50 MHz which means the period of the state exchange is 20 ns.

hits Q_2 at -0.188 V and the adiabatic swap process should be longer than 20 ns. At this stage, we realize the frequency of Q_2 and obtain a certain flux bias that is important in aSWAP technique.

3.2.2 Coupler characterization with aSWAP

The states between the coupler and Q_2 swap adiabatically only when the process of tuning the coupler is adiabatic and covers the whole anti-crossing point. In addition, the maximum frequency of the coupler is higher than that of the resonator. In order to avoid state exchange between the resonator and the coupler, the coupler should be tuned rapidly through the resonator region. Therefore, the aSWAP pulse is set to be in the shape of trapezoid. The coupler is on resonance with the resonator at -0.24 V bias (Figure 3.5b).

doi:10.6342/NTU202501389

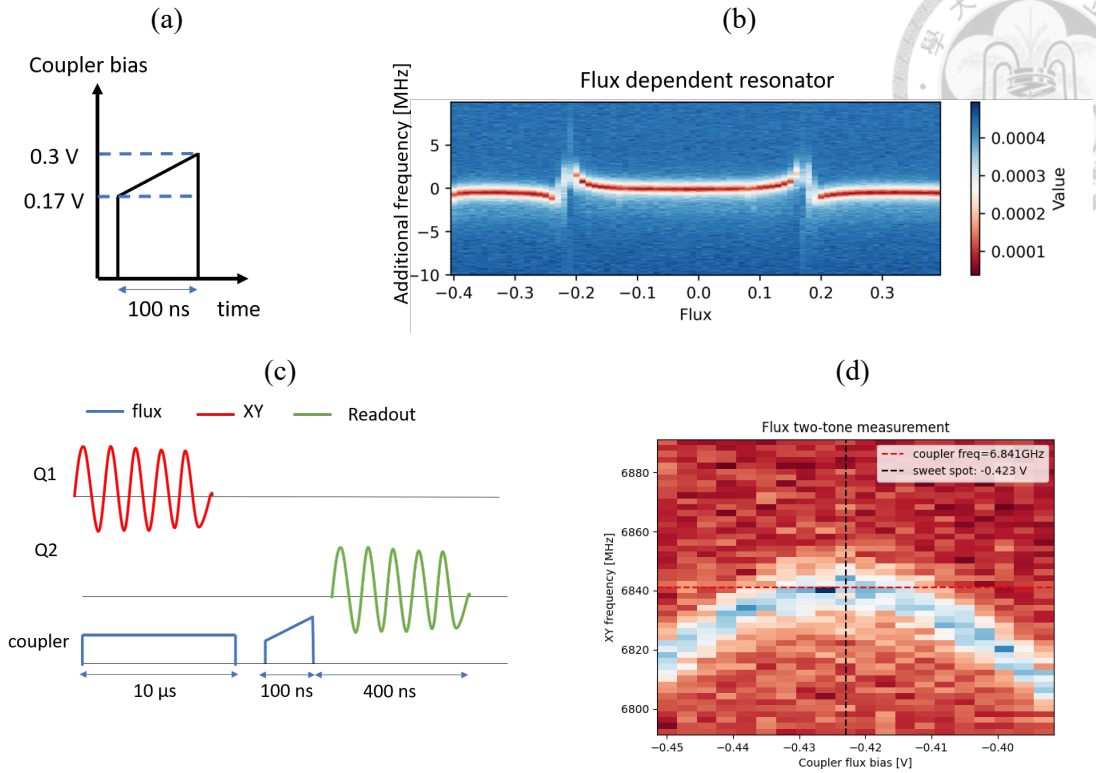

Figure 3.5: (a) The aSWAP pulse shape. (b) The result of flux dependent resonator with coupler's flux. The breakpoint means the coupler is on resonance with the resonator. There is one breakpoint at -0.24 V bias of the coupler. (c) The pulse sequence of the flux two-tone measurement adding the aSWAP pulse. (d)The result of the flux two-tone measurement for the coupler. The red color means the coupler stays in ground state, the blue represents the coupler is excited. The parabola of the coupler's frequency corresponding to its flux bias.

Therefore, the aSWAP pulse starting from -0.23 V to -0.1 V, step over 0.13 V in 100 ns (Figure 3.5a). Then, placing the aSWAP pulse before readout in any experiment which we did on qubits can let us measure the coupler like the qubit as usual. The flux two-tone measurement is taken as an example. Similarly to the pulse sequence in Figure 3.4a, but now the driving pulse in the XY line of Q_1 is used to excite the coupler, and the only change is to add a trapezoid-shaped pulse to the Z line of the coupler before readout, as shown in Figure 3.5c. From the result (Figure 3.5d) there is a blue parabola difference from the red background. This indicates that we can see the coupler spectrum corresponding to its magnetic flux bias successfully using the aSWAP technique.

doi:10.6342/NTU202501389

In order to know the frequency of the coupler far from the sweet spot, we sweep the pumping frequency of the driving pulse from 4.5 to 6.9 GHz and expand the bias to 0.4

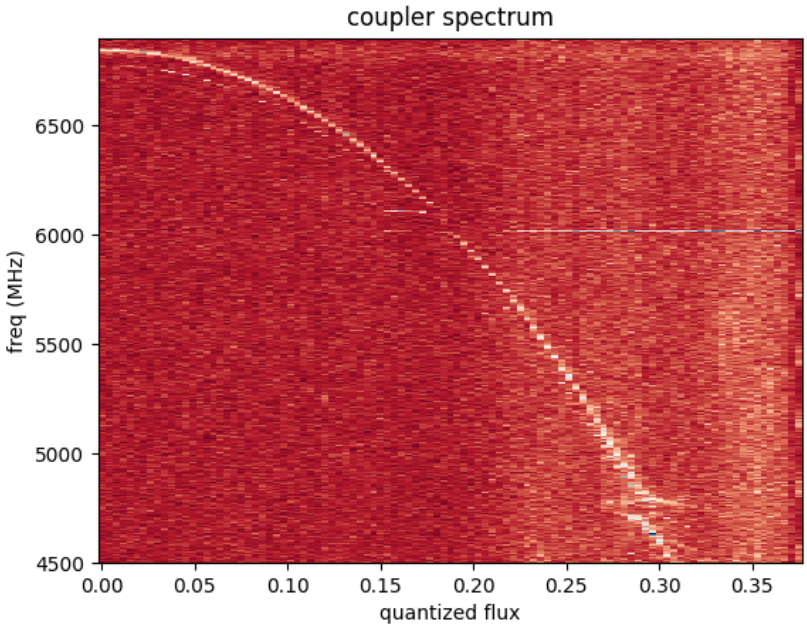

Figure 3.6: The extensive coupler spectrum corresponding to magnetic flux. The x-axis is transferred into the unit of quantized flux, the y-axis is driving frequency from 4.5 to 6.9 GHz. The white dots represent the coupler in excited state. In other words, the white dot at each bias denotes the corresponding frequency of the coupler.

quantized flux. The large spectrum of the coupler is shown in Figure 3.6. The parabola consists of the white dots that differ from the red background. There are some breakpoints along the white curve in the spectrum. There are two at 6.113 and 6.015 GHz representing the resonators next to the coupler. The other one at 4.749 GHz indicates that Q_2 beside the coupler, which is consistent with Figure 3.4b. Then, the power rabi and T1 measurement can be accomplished using the same method.

The power rabi measurement aims to calibrate an accurate π pulse by adjusting the amplitude of the XY pulse. The π pulse also called the $R_x(\pi)$ gate, which can transfer $|0\rangle$ to $|1\rangle$ and $|1\rangle$ to $|0\rangle$. The measurement starts with $|0\rangle$ and apply a Gaussian drag pulse pumping with the frequency of the coupler in the XY line of Q_1. Then we adjust the

doi:10.6342/NTU202501389

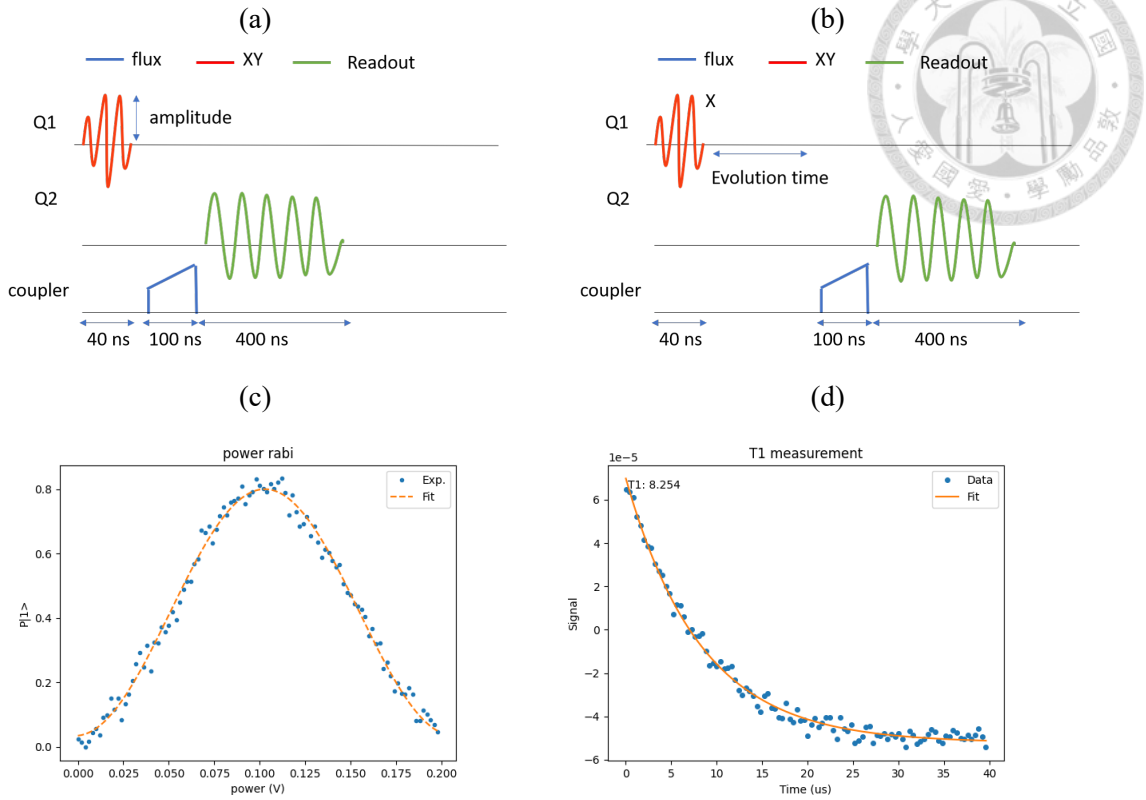

Figure 3.7: (a) The pulse sequence of the power rabi measurement of the coupler. (b) The pulse sequence of the T1 measurement of the coupler. (c) The result of the power rabi measurement. The power of the π pulse should be set to 0.1 V. (d) The result of the T1 measrement. Coupler's T1 is around 8.2 μs.

amplitude of the Gaussian drag pulse to find a certain power that maximizes the population of $|1\rangle$ (Figure 3.7a). If the coupler-Q_2 system stays in $|0\rangle \otimes |0\rangle$ initially, the state remains the same after aSWAP. Nevertheless, if the system stays in $|1\rangle \otimes |0\rangle$ initially, the state becomes $|0\rangle \otimes |1\rangle$ after aSWAP. Thus, the state of the coupler can be easily recognized as qubits. The result is shown in Figure 3.7c. So the amplitude of the π pulse for the coupler is set to 0.1 V.

The T1 measurement aims to find the decay rate of the transition from $|1\rangle$ to $|0\rangle$. First, apply a π pulse calibrated from the power rabi measurement. Then, alter the length of evolution time (Figure 3.7b. Identical to the case in the power rabi measurement, the state of the coupler can swap to Q_2 and read the population of $|1\rangle$ of the coupler via Q_2

doi:10.6342/NTU202501389

resonator.The fitting model is assumed to be an exponential decay.

$$\alpha e^{-t/T_1} + \beta \tag{3.1}$$

α, β are some constants and t is the evolution time after π pulse. The result in Figure 3.7d reveals that T_1 is around 8.2 μs.

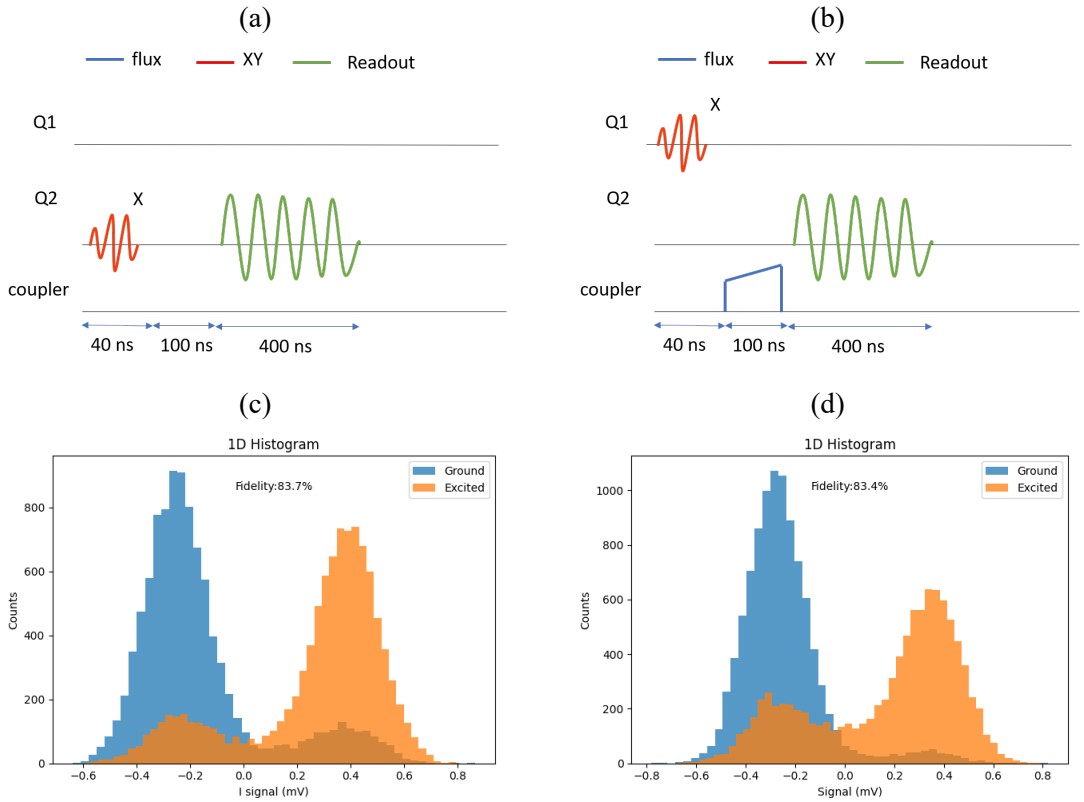

Figure 3.8: (a) The pulse sequence of the single shot measurement for Q_2. The dash line means prepare ground and excite separately. (b) The pulse sequence of the single shot measurement for the coupler. The dash line means prepare ground and excite separately. (c) The state distrubution of Q_2. The resulting readout fidelity is 83.7%. (d) The state distrubution of the coupler. The outcome readout fidelity is 83.4%, very close to the Q_2's.

Although the rabi experiment can calibrate the π pulse correctly, there is one way to examine it. Since Q_2 and the coupler share a resonator, the readout fidelity of the coupler should be measured roughly the same as Q_2. Therefore, we perform another experiment called single shot measurement to discriminate the state of Q_2 and the coupler. Prepare ground and excited state separately and then measure the state, count the population stay-

doi:10.6342/NTU202501389

ing in ground or excited to calculate the readout fidelity of Q_2 and the coupler. The final result shows that the readout fidelity of the coupler is close to that of Q_2 (Figure 3.8). Thus, it actually convinces us that the π pulse is calibrated correctly and that the T1, T2 measurement of the coupler that uses the π pulse is reliable.

3.3 CZ gate calibration

In the beginning, we characterize two qubits and one coupler in Q-C-Q systems. The parameters of the qubits and the coupler are listed in Table 3.1. The characterization of

	Q1	Q2	C
qubit frequency (GHz)	4.918	4.715	8.028
anharmonicity (MHz)	-206	-204	-152
T1 (μs)	6.2	9.3	5.7
T2 μs)	4.9	4.1	3.4

Table 3.1: Basic parameters of the qubits and the coupler at their sweet spot.

the coupler uses the method mentioned in 3.2. The next step to do is tuning the coupler to eliminate the ZZ-interaction between Q_1 and $Q2$.

3.3.1 ZZ-interaction minimization

Eq 2.4 tells that if $\omega_{11} \neq \omega_{01} + \omega_{10}$, there exists ZZ-interaction between two qubits. So, we can design the following experiment. Applying π pulse (X gate)and $\pi/2$ pulse ($X/2$) on Q_1 and Q_2 simultaneously, the state becomes $|1\rangle \otimes \frac{1}{\sqrt{2}}(|0\rangle - i|1\rangle)$. If the ZZ-interaction exists, ω_{01} shifts a little because of ω_{10}, Q_2 will rotate along the equator of the Bloch Sphere. The accumulated phase is exactly the frequency shift times the evolution time. Thus, we can obtain the ZZ-interaction by measuring the accumulated phase in real experiment and taking the derivative of the evolution time [8]. In addition, we can

doi:10.6342/NTU202501389

add another parameter to the experiment. Altering the flux bias of the coupler during the evolution time gives the information of the ZZ-interaction at different coupler's frequency. Finally, apply another $\pi/2$ pulse before readout to project the Bloch vector onto the z-axis of the Bloch Sphere since we can only measure the computational state. The complete pulse sequence is depicted in Figure 3.9a. The above plot in Figure 3.9b is the experimental

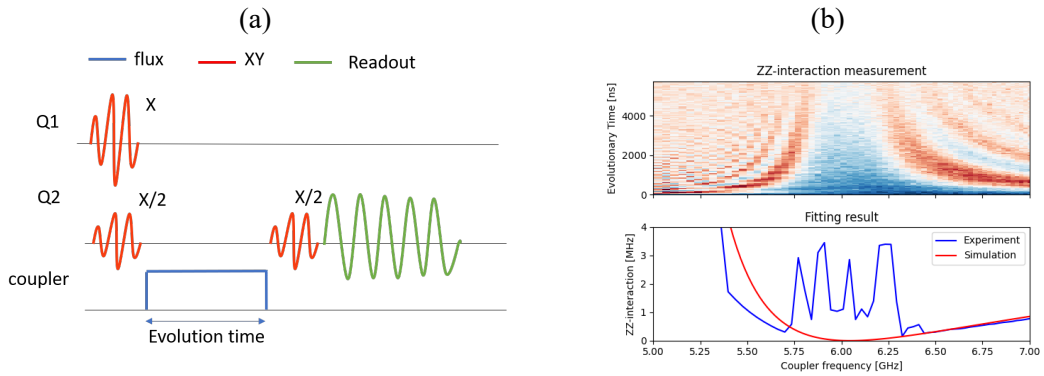

Figure 3.9: The ZZ-interaction measurement. (a) The pulse sequence. Apply X gate on Q_1 and X/2 on Q_2. If there is ZZ-interaction between two qubits, Q_2 will rotate along the equator of the Bloch Sphere during evolution time. The second X/2 on Q_2 is used to project the position on the equator to z-axis of the Bloch Sphere since we can only measure the computational state of qubits. (b) The above figure illustrates that Q_2 oscillate with different rate according to coupler's frequency. When the coupler is far detuned from the qubits, the ZZ-interaction increases slowly. On the contrary, when the coupler approaches closely to the qubits, the ZZ-interaction grows up instantly. The below figure is the fitting result of ZZ-interaction according to above figure. The blue line indicates the experimental data and the red represents the simulation result estimated by 2.8.

result and the bottom is the fitting result of the ZZ-interaction. The x-axis is transferred from flux bias to the corresponding frequency of the coupler. The red color in above figure means the ground state and the blue means the excited state. There are some slow oscillations on the right side of the figure and some fast oscillations on the left side. In the middle there exists a region which does not oscillate like others. The below figure is the fitting result according to the above figure. The ZZ-interaction in the region without oscillation corresponding to the above figure cannot be measured. The reason is that the T2 of the Q_2 is below $5\mu s$, which also means we can only measure the oscillation with

doi:10.6342/NTU202501389

frequency over 200 KHz .So, we have to utilize Eq 2.5 to 2.8 to simulate the residual ZZ-interaction beyond the limitation of the T2 of the qubit.

3.3.2 CZ gate construction

We construct the CZ gate with two magnetic square wave simultaneously (Figure 3.10). One is applied in the Z line of Q_2 in order to occur the state exchange between $|11\rangle$ and $|20\rangle$. The other is applied in the Z line of the coupler so as to increase the ZZ-interaction and accelerate the rate of the state exchange.

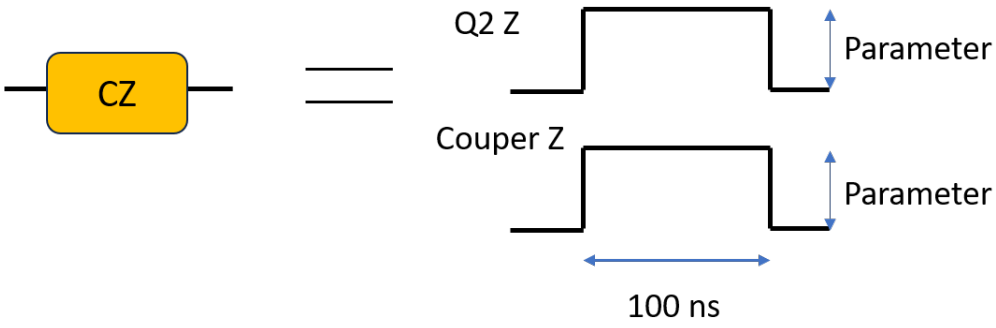

Figure 3.10: The concept of the CZ gate in the experiment. Our CZ gate consists of two short magnetic square waves. One applies on Q_2 for $|11\rangle$ and $20\rangle$ exchange, the other applies on the coupler to adjust the exchanging rate. We fix the wave length so that there are two parameters in our CZ gate that can be adjusted.

There are two flags for us to determine whether the CZ gate we constructed is good enough.

1. The population of four computational states after CZ gate
2. The conditional phase difference

First of all, we fix the wave length of two square waves to 100 ns. Then, there are two parameters, the amplitude of Q_2 Z determines the completeness of the state exchange and the amplitude of the coupler Z alters the speed of the state exchange. In order to find a certain pair of these parameters, we prepare $|11\rangle$ and then apply two square wave in the

doi:10.6342/NTU202501389

Z line of Q_2 and the coupler. Adjust the amplitude of two square waves and observe the readout signal on $Q2$ (Figure 3.11a). Since the state of $Q2$ swaps between $|1\rangle$ and $|0\rangle$, it is easy to recognize the state whether is $|11\rangle$ or $|20\rangle$. The blue color in Figure 3.11b indicates the excited state and the red represents the ground state. Since the $|11\rangle$ returned is the key point, we need to focus on the blue region. The range of parameter adjustment reduces according to Figure 3.11b and is convenient for the following experiments.

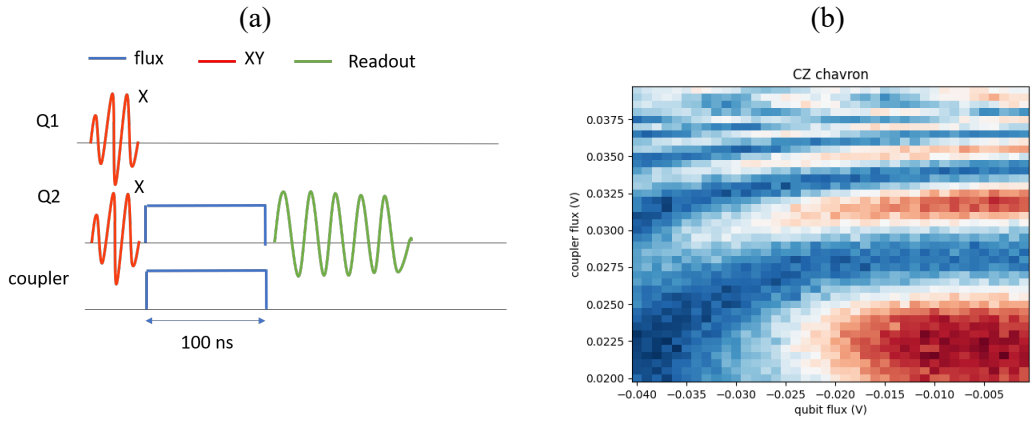

Figure 3.11: The CZ chavron experiment. (a) The pulse sequence. Apply X gate on Q_1 and Q_2 to prepare $|11\rangle$ initially. Then insert two square waves after X gate and adjust the amplitudes. Readout Q_2 since it swaps between $|1\rangle$ and $|0\rangle$. (b) The figure illustrates that Q_2 swapping relative to the amplitude of square wave on the coupler. The horizontal axis is the amplitude of magnetic square wave of Q_2 and the vertical axis is that of the coupler. The blue color indicates $|11\rangle$ and the red represents $|20\rangle$.

After picking up a pair of pararmeters based on Figure 3.11b, then perform a detailed examination of the population in four computational states. The experimental concept is that the population of four computational states remain unchanged through the CZ gate. Thus, we also prepare $|11\rangle$ first, then follow with or without two magnetic square waves fixed in 100 ns and decided amplitudes, readout Q_1 and Q_2 in the end (Figure 3.12a). There are four computational states for two qubits, so the result should present the populations in those computational states (Figure 3.12b). If the distribution of the population in four states varies through the CZ gate, it is essential to choose another pair of parameters

doi:10.6342/NTU202501389

according to Figure 3.11b.

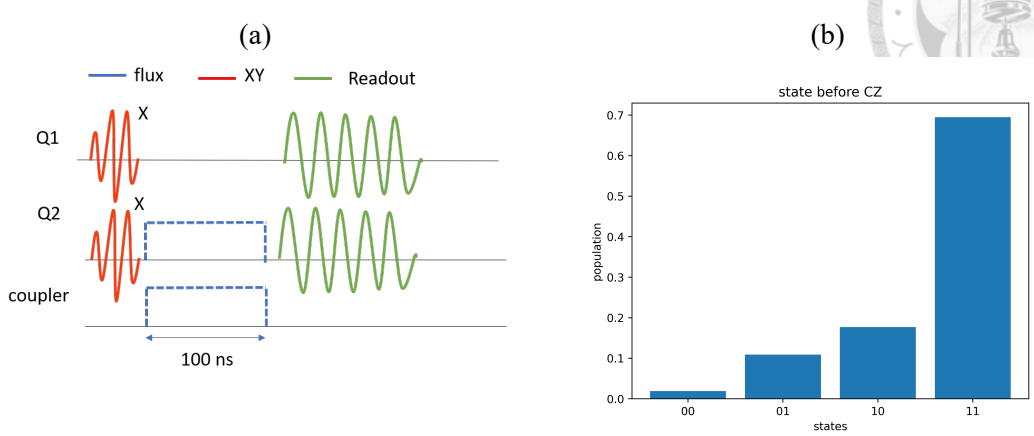

Figure 3.12: The population of $|11\rangle$ experiment. (a) The pulse sequence. Apply X gate on Q_1 and Q_2 to prepare $|11\rangle$ initially. Following with or without the CZ gate. Readout both Q_1 and Q_2 simultaneously to discriminate the population of four computational states for two-qubit. (b) The schematic result of the experiment. If the distribution of the population of four computational states remains the same after CZ gate, the parameters is a good pair for constructing CZ gate.

After completing the first flag, the next examination is to check the phase of the returned $|11\rangle$. We prepare two states separately. Applying $X/2$ on Q_2 gets $\frac{|00\rangle - i|01\rangle}{\sqrt{2}}$ and applying X on Q_1, $X/2$ on Q_2 obtains $\frac{|10\rangle - i|11\rangle}{\sqrt{2}}$. Then follow with two magnetic square waves fixed in 100 ns and decided amplitudes. According to Eq 2.9 and 2.10, $|00\rangle$, $|01\rangle$ and $|10\rangle$ remain themselves through the CZ gate, but $|11\rangle$ has another minus sign. If the CZ gate is constructed successfully, those two states become $\frac{|00\rangle - i|01\rangle}{\sqrt{2}}$ and $\frac{|10\rangle + i|11\rangle}{\sqrt{2}}$. After projected on the computational basis of Q_2 by another $X/2$, the phase difference of $\frac{|0\rangle - i|1\rangle}{\sqrt{2}}$ and $\frac{|0\rangle + i|1\rangle}{\sqrt{2}}$ emerges and the value is π. In order to present the phase difference clearly, we give the second $X/2$ extra virtual rotational Z gate, $R_z(\theta)$, from $\theta = 0$ to $\theta = 2\pi$ (Figure 3.13a). Then the result shows two sinusoidal curves with a phase difference of π (Figure 3.13b). If the phase difference measured far from π, the amplitude of two square waves should be adjusted again.

After conforming to two flags with certain parameters of two square waves, the CZ

doi:10.6342/NTU202501389

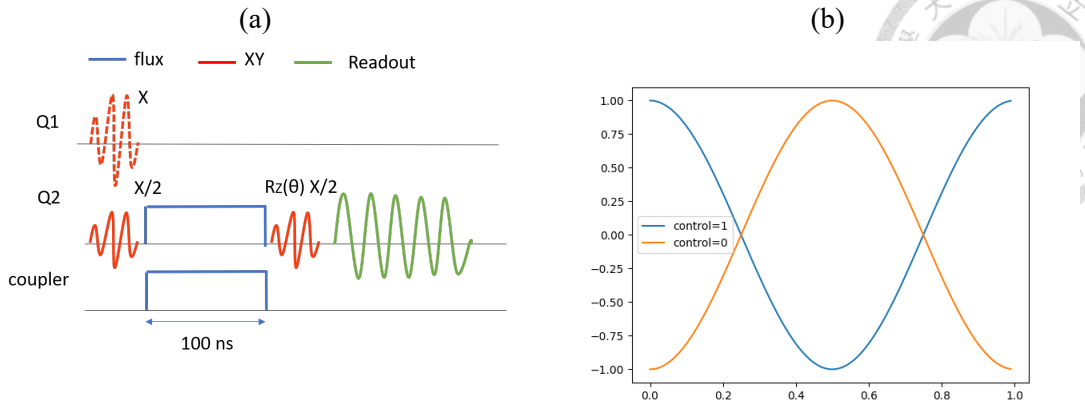

Figure 3.13: The conditional phase difference measurement. (a) The pulse sequence. Apply X/2 on Q_2 to prepare $|0\rangle \otimes \frac{|0\rangle - i|1\rangle}{\sqrt{2}}$ initially. Insert the CZ gate. Apply virtual rotational Z gate and X/2 to make the phase difference clearly. Repeat this experiment again but with an X gate on Q_1 so the state becomes $|1\rangle \otimes \frac{|0\rangle - i|1\rangle}{\sqrt{2}}$ initially. The dash line on X gate means this experiment need the comparison with or without the X gate on Q_1. (b) The ideal case of the result. Since the CZ gate add an extra phase π on $|11\rangle$, it is expected to observe the two curve with phase difference π from the result. The horizontal axis is in the unit of 2π.

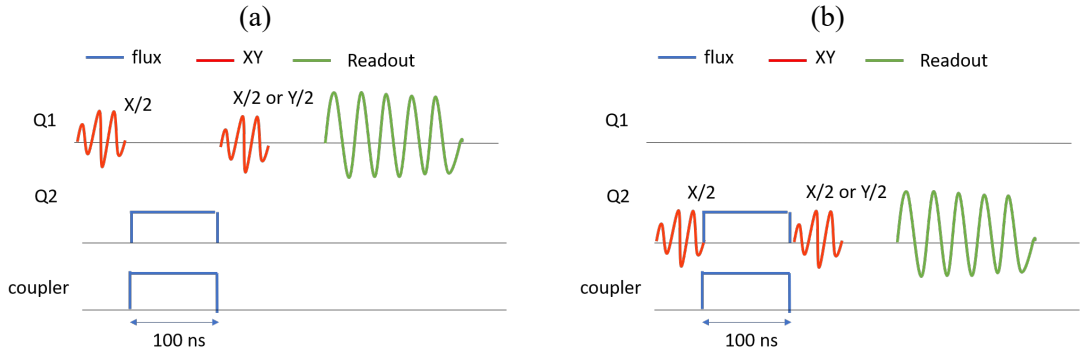

Figure 3.14: The pulse sequence of CZ phase compensation (a) on Q_1 (b) on Q_2.

gate is roughly established. Since the qubits and the couplers are tunable by magnetic flux, the phase of the quantum state shifts when it feels some extra magnetic flux. For the purpose of correcting this phenomenon, we should give a phase compensation after our CZ gate. We apply $X/2$ to Q_1 to prepare $\frac{|0\rangle - i|1\rangle}{\sqrt{2}} \otimes |0\rangle$. Then, passing through a CZ gate makes the state become $\frac{|0\rangle - e^{-i(\pi/2+\phi)}|1\rangle}{\sqrt{2}} \otimes |0\rangle$. The factor ϕ is the phase that needs to compensate. The value can be obtained by applying $X/2$ and $Y/2$ after the CZ gate to project the x axis and the y axis to the z axis (Figure 3.14a. We give a virtual rotational Z gate with specific ϕ after the CZ gate to rotate the Bloch Sphere and align its axis with the state.

doi:10.6342/NTU202501389

Consequently, the state before the CZ gate remains the same relative to the Bloch Sphere after the compensation. Q_2 also requires compensation after the CZ gate. Therefore, repeat the same experiment performed on Q_1 to Q_2 (Figure 3.14b. After receiving two compensating values for each qubit, the CZ gate is successfully constructed.

3.4 Two-Qubit RB

The code of two-qubit randomized benchmarking is written by Quantum Machine. Therefore, we just put the parameters of the CZ gate in the code. Finally, it is necessary to determine the circuit depth m, k type of different circuits for each m and n shots for each circuit. The code starts with baking two-qubit Cliffords from six single-qubit gates $\{X, Y, X/2, Y/2, -X/2, -Y/2\}$ and CZ gate calibrated manually. Then, randomly choose the gates from the baking Cliffords to build some circuits according to the parameters {m,k} mentioned above. Finally, measure the state of two qubits simultaneously to observe the population in $|00\rangle$ and plot the curve relative to different circuit depths m. Fitting the curve with exponential decay obtains the value of two-qubit fidelity.

doi:10.6342/NTU202501389

doi:10.6342/NTU202501389

Chapter 4

Experimental Result

We tune the frequency of the coupler to 6.22 GHz to turn off the ZZ-interaction between Q_1 and Q_2. From the simulation result, there still exists a 100 KHz ZZ-interaction

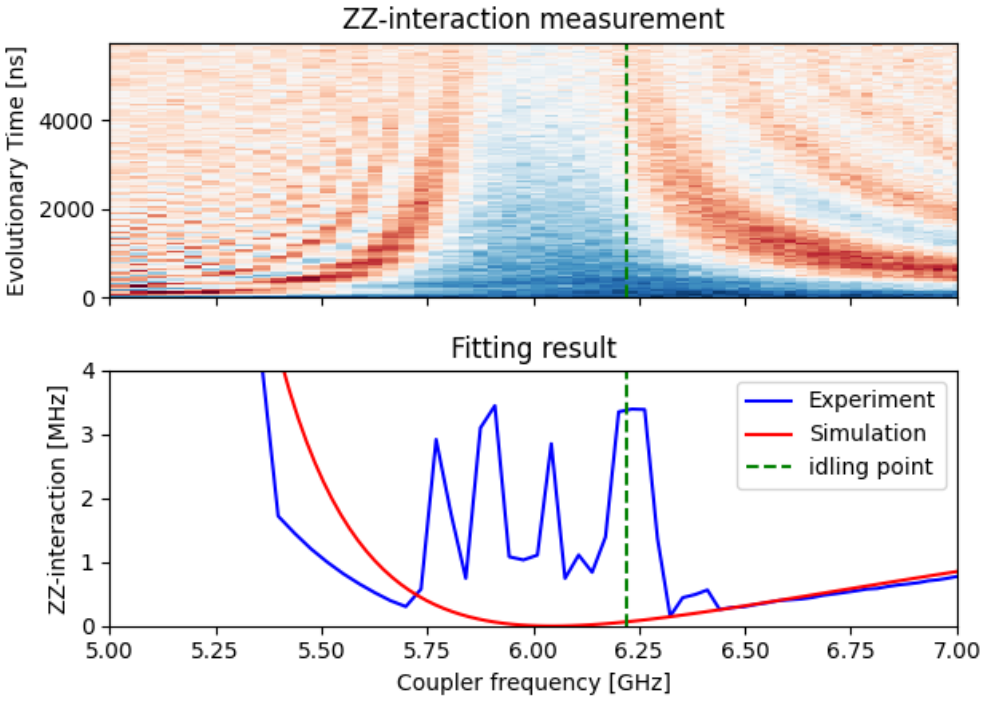

Figure 4.1: We tune the coupler to 6.22 GHz (green dash line) to turn off the ZZ-interaction between Q_1 and Q_2. Due to the limitation of T2 of Q_2, the fitting result of ZZ-interaction is messy in the region of 5.75 GHz to 6.25 GHz. From the simulation curve, there still exists roughly 100 kHz ZZ-interaction between Q_1 and Q_2.

doi:10.6342/NTU202501389

between two qubits. The reason for not tuning downward is that the resonator's frequency is about 6.1 GHz so that the coupler is too close to the resonator. It will seriously decrease the readout fidelity for two qubits and affect the discrimination to the state of qubits.

After finding an idling point for the coupler, we characterize the Q-C-Q system again. The basic parameters of two qubits and one coupler are listed below:

	Q1	Q2	C
qubit frequency (GHz)	4.918	4.715	6.22
anharmonicity (MHz)	-206	-204	-152
T1 (μs)	6.2	9.3	1.5
T2 μs)	4.9	4.1	0.7

Table 4.1: Basic parameters of the qubits and the coupler at idling point.

Then, we tune Q_2 and the coupler for 100 ns simultaneously by different amplitudes of magnetic flux. The resulting figure shows that the range (-0.025, 0.0) for Q_2, (0.025, 0.03)

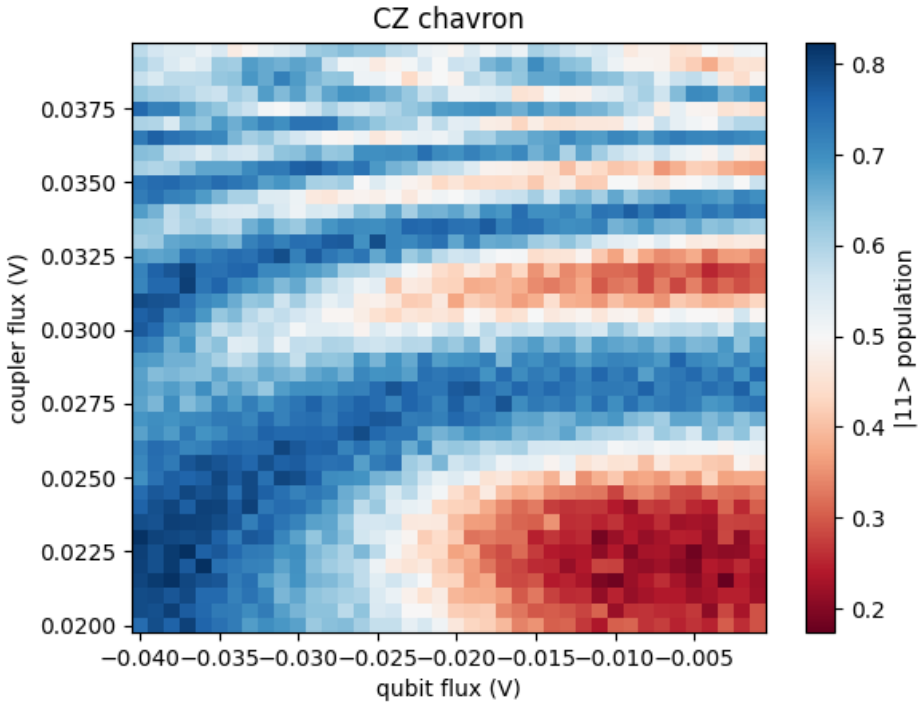

Figure 4.2: CZ chavron relative to the amplitude of qubit's and coupler's magnetic flux. The colorbar on the right side indicates that the blue area has more population in $|11\rangle$. The (Q,C) pair we need locates in the range (-0.03-0.0, 0.025-0.03) since it is the first returning $|11\rangle$ along the vertical axis.

doi:10.6342/NTU202501389

for the coupler are possible to achieve CZ gate since blue represents $|11\rangle$. After trying few pairs of parameters, we find a suitable pair (-0.004, 0.028) whose population of four

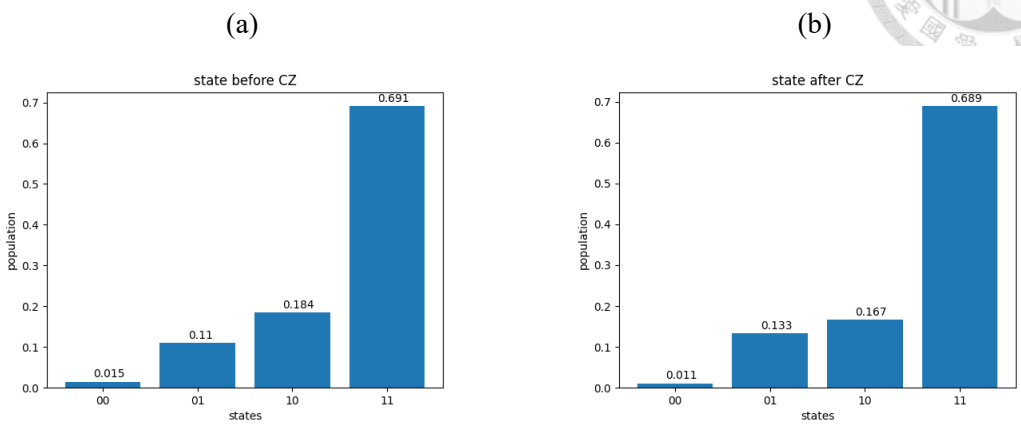

Figure 4.3: The population of four computational states with the pair (-0.004, 0.028). (a) before CZ gate. (b) After CZ gate. The populations of $|11\rangle$ are almost the same and the population of other states not much difference comparing to the population before CZ gate. Therefore, this pair is good enough for CZ gate construction.

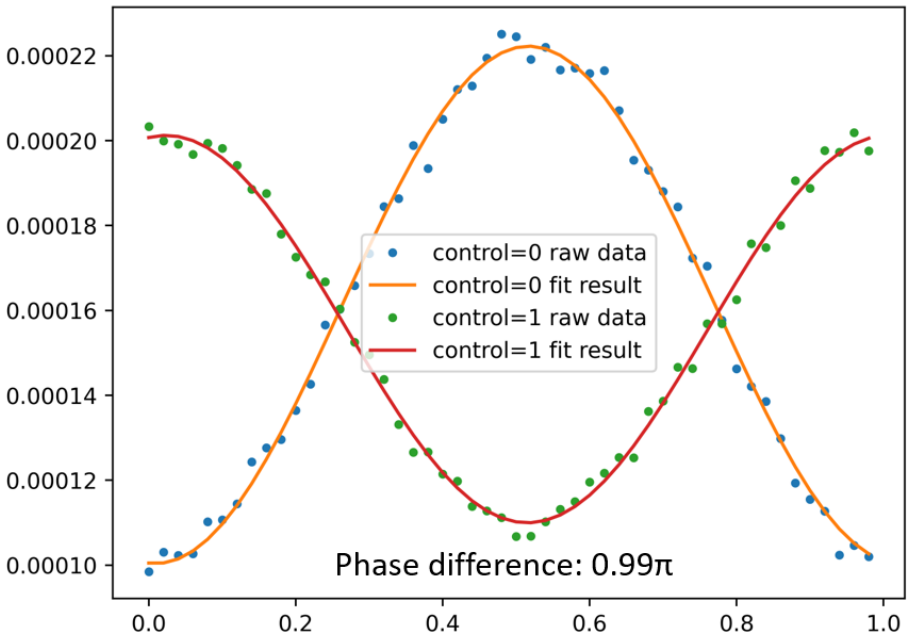

Figure 4.4: The result of the phase difference with the pair (-0.004, 0.028). The fitting result shows that the phase difference between control at 0 and control at 1 is almost a π.

computational states remains almost the same after CZ gate and the conditional phase difference reaches almost π. In the last step of CZ gate construction, we obtain Q_1 need to

doi:10.6342/NTU202501389

compensate 1.7 rad and Q_2 need to compensate -3.07 rad. Finally, we put the parameters

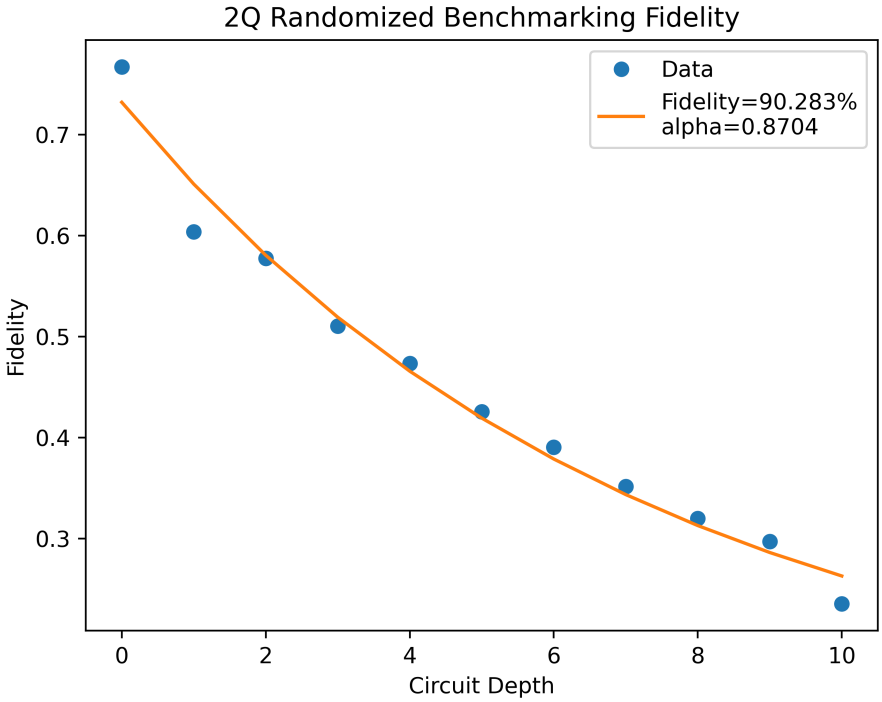

Figure 4.5: The result of two-qubit randomized benchmarking. The fidelity of per two-qubit Clifford gate is 90.283% from the exponential fitting.

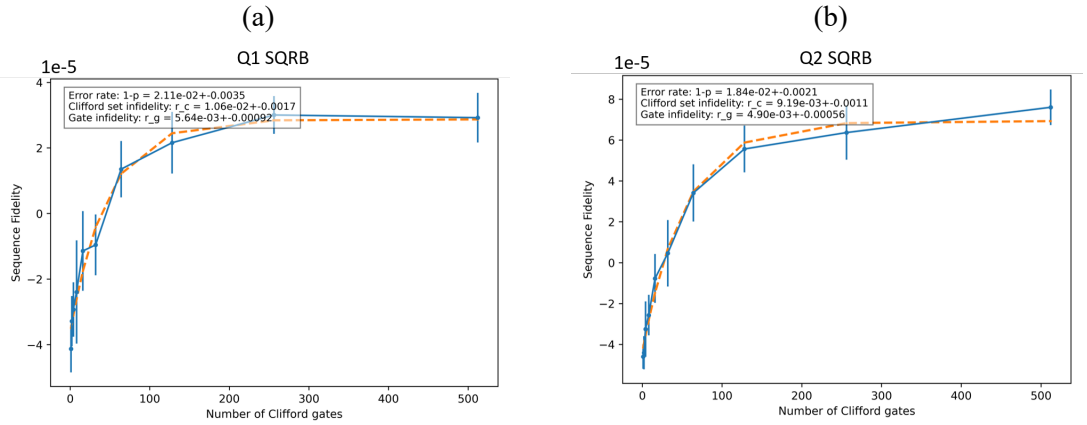

Figure 4.6: The result of single qubit randomized benchmarking. (a) The error per single qubit gate for Q_1, $r_{SQ,\,Q_1} = 5.64 \times 10^{-3}$. (b) The error per single qubit gate for Q_2, $r_{SQ,\,Q_2} = 4.9 \times 10^{-3}$

of CZ gate above into the two-qubit randomized benchmarking measurement and set the circuit depths from 1 to 10, for each circuit depth generates 10 types of sequence, for each sequence measure 1000 shots. The fitting result shows that the fidelity of per two-qubit

doi:10.6342/NTU202501389

Clifford gate is 90.2%. According to Eq 2.19, the error of one CZ gate can be calculated by the error of per two-qubit Clifford gate and single qubit gate. The single qubit gate error $r_{SQ,\,Q_1} = 5.64 \times 10^{-3}$, $r_{SQ,\,Q_2} = 4.9 \times 10^{-3}$. We take the average to represent the error of single qubit gate so that $r_{SQ} = 5.27 \times 10^{-3}$. Then, the error per CZ gate can be calculated through Eq 2.19, $r_{CZ} = 3.6 \times 10^{-2}$. The coherence limit for CZ gate [9, 10] can be estimated by T1 and dephasing time of qubits. By measuring the T1 and dephasing time when CZ gate is operating, the coherence limit for CZ gate $r_{CZ}^{limit} = 2.3 \times 10^{-2}$. This value can be compared with the experimental measured CZ gate error obtained above, which is a little higher than the limit.

doi:10.6342/NTU202501389

doi:10.6342/NTU202501389

Chapter 5

Conclusion

We demonstrate a full process of characterizing the coupler without dedicated resonator and calibrating the CZ gate with tunable coupler. Although the error of per CZ gate resulting from TQRB is just a little higher than the coherence limit, there are more things to do that can improve the fidelity. One is about the frequency of the coupler that turns off the ZZ-interaction. According to the simulation result, it should be tuned downward to around 6.1 GHz which really eliminates the ZZ-interaction between two qubits. But 6.1 GHz is too close to the resonator, then we should tune up the coupler to some place while measuring the state of qubits. This method will sacrifice the readout fidelity but improve the gate fidelity. The other point is that we use square wave to tune the frequency of the qubits and the coupler up and down instantaneously. This process is non-adiabatic and causes flux distortion of the qubits and the coupler. Therefore, modifying the edge of the magnetic wave to be adiabatic is necessary in the future.

doi:10.6342/NTU202501389

doi:10.6342/NTU202501389

References

[1] Xuan Zhang, Xu Zhang, Changling Chen, Kai Tang, Kangyuan Yi, Kai Luo, Zheshu Xie, Yuanzhen Chen, and Tongxing Yan. Characterization and optimization of tunable couplers via adiabatic control in superconducting circuits, 2025.

[2] Daniel Grier and Luke Schaeffer. The Classification of Clifford Gates over Qubits. Quantum, 6:734, June 2022.

[3] Fabian Marxer, Antti Vepsäläinen, Shan W. Jolin, Jani Tuorila, Alessandro Landra, Caspar Ockeloen-Korppi, Wei Liu, Olli Ahonen, Adrian Auer, Lucien Belzane, Ville Bergholm, Chun Fai Chan, Kok Wai Chan, Tuukka Hiltunen, Juho Hotari, Eric Hyyppä, Joni Ikonen, David Janzso, Miikka Koistinen, Janne Kotilahti, Tianyi Li, Jyrgen Luus, Miha Papic, Matti Partanen, Jukka Räbinä, Jari Rosti, Mykhailo Savytskyi, Marko Seppälä, Vasilii Sevriuk, Eelis Takala, Brian Tarasinski, Manish J. Thapa, Francesca Tosto, Natalia Vorobeva, Liuqi Yu, Kuan Yen Tan, Juha Hassel, Mikko Möttönen, and Johannes Heinsoo. Long-distance transmon coupler with cz-gate fidelity above 99.8%. PRX Quantum, 4:010314, Feb 2023.

[4] Peng Zhao, Dong Lan, Peng Xu, Guangming Xue, Mace Blank, Xinsheng Tan, Haifeng Yu, and Yang Yu. Suppression of static zz interaction in an all-transmon quantum processor. Phys. Rev. Appl., 16:024037, Aug 2021.

doi:10.6342/NTU202501389

[5] Youngkyu Sung, Leon Ding, Jochen Braumüller, Antti Vepsäläinen, Bharath Kannan, Morten Kjaergaard, Ami Greene, Gabriel O. Samach, Chris McNally, David Kim, Alexander Melville, Bethany M. Niedzielski, Mollie E. Schwartz, Jonilyn L. Yoder, Terry P. Orlando, Simon Gustavsson, and William D. Oliver. Realization of high-fidelity cz and zz-free iswap gates with a tunable coupler. Phys. Rev. X, 11:021058, Jun 2021.

[6] Easwar Magesan, Jay M. Gambetta, B. R. Johnson, Colm A. Ryan, Jerry M. Chow, Seth T. Merkel, Marcus P. da Silva, George A. Keefe, Mary B. Rothwell, Thomas A. Ohki, Mark B. Ketchen, and M. Steffen. Efficient measurement of quantum gate error by interleaved randomized benchmarking. Physical Review Letters, 109(8), August 2012.

[7] Rami Barends, Julian Kelly, Anthony Megrant, Andrzej Veitia, Daniel Thomas Sank, Evan Jeffrey, Theodore White, Josh Mutus, Austin G. Fowler, Brooks Campbell, You Lung Chen, Zijun Chen, Benjamin Chiaro, Andrew Dunsworth, Charles J. Neill, P. OMalley, Pedram Roushan, Amit Vainsencher, James Wenner, Alexander N. Korotkov, Andrew N. Cleland, and John M. Martinis. Superconducting quantum circuits at the surface code threshold for fault tolerance. Nature, 508:500–503, 2014.

[8] Zhongchu Ni, Sai Li, Libo Zhang, Ji Chu, Jingjing Niu, Tongxing Yan, Xiuhao Deng, Ling Hu, Jian Li, Youpeng Zhong, Song Liu, Fei Yan, Yuan Xu, and Dapeng Yu. Scalable method for eliminating residual zz interaction between superconducting qubits. Phys. Rev. Lett., 129:040502, Jul 2022.

[9] Ji Chu and Fei Yan. Coupler-assisted controlled-phase gate with enhanced adiabaticity. Phys. Rev. Appl., 16:054020, Nov 2021.

doi:10.6342/NTU202501389

[10] Tahereh Abad, Jorge Fernández-Pendás, Anton Frisk Kockum, and Göran Johansson. Universal fidelity reduction of quantum operations from weak dissipation. Physical Review Letters, 129(15), October 2022.

doi:10.6342/NTU202501389